J Neurophysiol 97: 2107–2120, 2007.
First published January 3, 2007; doi:10.1152/jn.00405.2006.

BOLD Coherence Reveals Segregated Functional Neural Interactions When Adapting to Distinct Torque Perturbations

Eugene Tunik,[1,2] Paul J. Schmitt,[1] and Scott T. Grafton[1,3]

[1]*Department of Psychological and Brain Sciences, Center for Cognitive Neuroscience, Dartmouth College, Hanover, New Hampshire;* [2]*Department of Physical Therapy, Steinhardt School of Education, New York University, New York, New York; and* [3]*Department of Psychology, Sage Center for the Study of the Mind, University of California–Santa Barbara, Santa Barbara, California*

Submitted 17 April 2006; accepted in final form 15 December 2006

Tunik E, Schmitt PJ, Grafton ST. BOLD coherence reveals segregated functional neural interactions when adapting to distinct torque perturbations. *J Neurophysiol* 97: 2107–2120, 2007. First published January 3, 2007; doi:10.1152/jn.00405.2006. In the natural world, we experience and adapt to multiple extrinsic perturbations. This poses a challenge to neural circuits in discriminating between different context-appropriate responses. Using event-related fMRI, we characterized the neural dynamics involved in this process by randomly delivering a position- or velocity-dependent torque perturbation to subjects' arms during a target-capture task. Each perturbation was color-cued during movement preparation to provide contextual information. Although trajectories differed between perturbations, subjects significantly reduced error under both conditions. This was paralleled by reduced BOLD signal in the right dentate nucleus, the left sensorimotor cortex, and the left intraparietal sulcus. Trials included "NoGo" conditions to dissociate activity related to preparation from execution and adaptation. Subsequent analysis identified perturbation-specific neural processes underlying preparation ("NoGo") and adaptation ("Go") early and late into learning. Between-perturbation comparisons of BOLD magnitude revealed negligible differences for both preparation and adaptation trials. However, a network-level analysis of BOLD coherence revealed that by late learning, response preparation ("NoGo") was attributed to a relative focusing of coherence within cortical and basal ganglia networks in both perturbation conditions, demonstrating a common network interaction for establishing arbitrary visuomotor associations. Conversely, late-learning adaptation ("Go") was attributed to a focusing of BOLD coherence between a cortical–basal ganglia network in the viscous condition and between a cortical–cerebellar network in the positional condition. Our findings demonstrate that trial-to-trial acquisition of two distinct adaptive responses is attributed not to anatomically segregated regions, but to differential functional interactions within common sensorimotor circuits.

INTRODUCTION

Effective movement necessitates adaptation to perturbations to the sensorimotor system. Whether different neural circuits in the human brain underlie the nervous system's capability to flexibly adapt to various perturbations remains unknown. Although numerous imaging studies have investigated circuits involved in sensorimotor remapping, only a handful have addressed adaptation to torque perturbations. Early positron emission tomography (PET) studies of two-dimensional (2D) reaching under viscous resistance revealed a learning-dependent increase in regional cerebral blood flow (rCBF) to the left dorsolateral prefrontal (DLPFC) cortex and the bilateral putamen that, on retention testing, was reduced in the DLPFC but increased in the left posterior parietal, dorsal premotor, and right anterior cerebellar cortices (Nezafat et al. 2001; Shadmehr and Holcomb 1997, 1999). Recruitment of frontal–parietal, basal ganglia, and cerebellar networks is consistent with a breadth of studies using various visuomotor learning/calibration paradigms (Desmurget et al. 2000; Floyer-Lea and Matthews 2004; Ghilardi et al. 2000; Graydon et al. 2005; Imamizu et al. 2000; Inoue et al. 2000; Krakauer et al. 2004; Martin et al. 1996; Miall and Jenkinson 2005; Smith and Shadmehr 2005) implicating these areas in forming specific functional interactions for adaptive motor control.

The degree of anatomical and functional segregation within this network for different forms of adaptation remains poorly understood. A recent blocked functional magnetic resonance imaging (fMRI) study partly addressed the issue of anatomical specificity to on-line error detection/correction as subjects made 2D reaching movements during directionally inconsistent viscous and visual perturbations (Diedrichsen et al. 2005). The authors noted negligible anatomical segregation between regions activated for "kinematic" and "dynamic" perturbations—that is, the motor cortex, secondary somatosensory cortex, a region along the postcentral sulcus, area 5, and cerebellar lobules V and VIII. Although novel and interesting, the blocked nature of their design did not allow for analysis of functional neural interactions and, although the use of inconsistent perturbations addressed on-line control, they could not attest to issues related to adaptation.

We thus used an event-related fMRI design to investigate whether distinct functional interactions, rather than anatomical segregation, might underlie acquisition of different adaptive behaviors. Subjects performed a target-capture task while adapting to randomly presented position- or velocity-dependent torque perturbations. Unlike the study of Diedrichsen et al. (2005), we kept the mapping between cursor and forearm movement constant (thus avoiding issues pertaining to kinematic vs. dynamic adaptation) but instead manipulated the torque perturbation to the forearm. We expected that any learning associated with the task should be attributed to temporal changes in neural activation patterns. We also hypothesized that if subjects showed evidence of developing perturbation-specific control policies, then this too should be reflected in neural activation—either by the involvement of distinct

Address for reprint requests and other correspondence: S. T. Grafton, Department of Psychology, Sage Center for the Study of the Mind, Building 251, Room 3837, UC Santa Barbara, Santa Barbara, CA 93106-9660 (E-mail: grafton@psych.ucsb.edu).

The costs of publication of this article were defrayed in part by the payment of page charges. The article must therefore be hereby marked "*advertisement*" in accordance with 18 U.S.C. Section 1734 solely to indicate this fact.

anatomical regions for each perturbation condition or by the involvement of distinct *functional interactions* among common regions. We tested these two predictions by analyzing the imaging data using standard subtraction techniques (which would reveal anatomical segregation) and by comparing the blood oxygenation level–dependent (BOLD) signal coherence between common distributed sensorimotor regions (which would reveal distinct functional interactions). We suspected that the anatomical recruitment of cortical and subcortical sensorimotor regions for adaptation to position- and velocity-dependent perturbations should be rather similar, in part based on the finding of Diedrichsen et al. (2005) of modest differences in anatomical segregation between adaptation for kinematic versus dynamic perturbations. However, we hypothesized that a comparison of trial-to-trial BOLD coherence across a set of brain regions for the two types of perturbations might reveal distinct functional neural interactions at the network level.

We investigated two issues. First, we asked whether specificity in functional interactions would be observed during movement preparation versus adaptation. For this, we provided subjects with a perturbation-specific cue during a preparatory period, followed by a "NoGo" (*preparation trials*) or "Go" (*preparation + adaptation trials*) signal. We hypothesized that contextual cuing during preparation engages only common functional circuits related to arbitrary visuomotor association processes but implementation of the adaptive strategy (prepare and adapt) necessitates perturbation specificity. Second, we investigated learning-dependent changes in functional interactions. We hypothesized that preparation and adaptation in the latter stage of the learning process would be associated with a relative increase in coherence within a focused set of neural regions involving the frontoparietal cortex, cerebellum, and basal ganglia.

METHODS

Subjects

Fifteen right-handed (Oldfield 1971) individuals (mean age ± SD; 24.7 ± 3.7; 11 females, four males) with no history of neurological impairment participated after signing informed institutional consent.

Setup and procedure

Subjects held a handle connected by a 10-ft. (3.05 m) Delrin rod to a torque motor (Model #SM233BEN16N, Parker Automation), secured against the wall in the scanning suite (Fig. 1*A*).

A semipronated forearm orientation was calibrated as 0° with a 1:1 correspondence between forearm rotation and cursor revolution about a central point (*C*) on the display. Each trial was composed of four epochs (Fig. 1*A*).

1) Epoch a: Cursor alignment over the start target (Tf), located at one of four randomly specified locations (20, 40, 60, or 80°).

2) Epoch b: Preparing an out and back movement from Tf to a target (Tr), always −90° from Tf, and back to Tf (2 s). The targets' respective colors (blue, red) served as perturbation-specific contextual cues (positional, viscous). White targets always represented a null torque field.

3) Epoch c: "Go" trial (75% of trials): out and back movement to the remembered targets cued by the disappearance of the cursor and targets; or "NoGo" trial (25%): remain motionless over Tf cued by a central red cross.

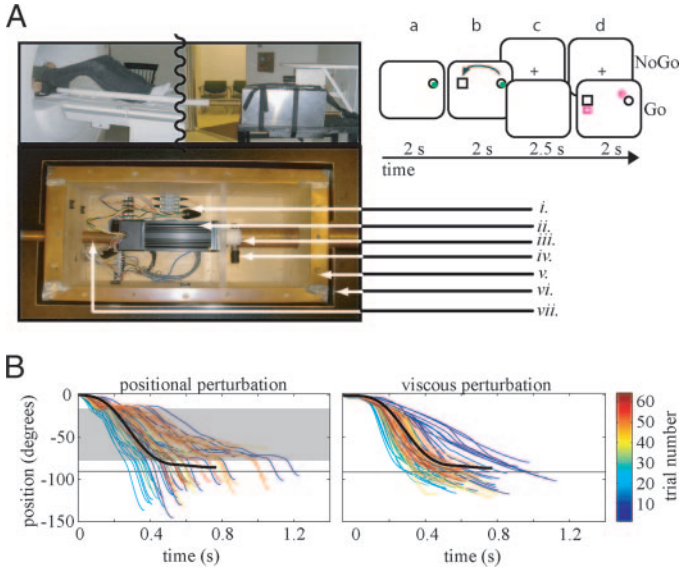

FIG. 1. *A*: experimental setup and event timing (see METHODS for description of epochs *a*, *b*, *c*, *d*). Arrow in epoch *b* schematizes the cursor trajectory from Tf to Tr that would occur in the go trials of epoch *c*. An enlarged view of the inside of the shielded box housing the motor components: (*i*) wiring for the motor and encoder with fuses; (*ii*) motor and encoder; (*iii*) copper outlet for the Delrin shaft attached to the motor; (*iv*) safety bolt to prevent full rotation; (*v*) copper-shielded box (top removed) attached to an inner wooden frame; (*vi*) outer MUMETAL nesting box (top removed); (*vii*) copper outlet for the cables, which remain shielded until reaching the control room (see METHODS). *B*: representative subject's outward trajectories in the positional and viscous conditions. Thick black trajectory shows the mean of the last 5 null-1 trials. Thin horizontal line marks the target. Gray area depicts the range within which the positional perturbation was enabled.

4) Epoch d: Knowledge of results of error at reversal (Sr) and final (Sf) position. Peak velocity was also provided as a small unitless bar in the corner of the display to encourage fast movement.

The cycle from the start of one trial to the start of a subsequent trial consisted of: 2 s to allow the subject to align the cursor to the start position, 2 s to allow the subject to view the target positions, a maximum of 2.5 s for movement execution, and 2 s for knowledge of results. After the end of the feedback epoch, a new start position was immediately specified and a new trial cycle began.

Perturbations and training

Subjects first trained on a *null* perturbation (motor disabled) for 60 trials (null-1). Immediately afterward they were exposed for 160 trials to one of two equally probable perturbations, presented in a random fashion. One perturbation type was a position-dependent perturbation (100 oz-in. [0.8 Nm] torque in the clockwise direction) enabled if the handle orientation was within ±31.5° from the midway angle between vectors $\overrightarrow{CTf}$ and $\overrightarrow{CTr}$ (torque-field range, 63°). Note that our use of the term "positional" refers to this step torque that was enabled and disabled when the specified position was reached. Note too that because subjects' movements were bidirectional (a counterclockwise out movement and a clockwise return movement) and because the positional perturbation was unidirectional in the clockwise direction, the perturbation was resistive to the subjects' "out" movement component but assistive for the return component. The other was a velocity-dependent perturbation, a positive viscous torque proportional to the subjects' velocity (−0.5 oz-in.·deg^{-1}·s^{-1} [0.004 Nm·deg^{-1}·s^{-1}]). Given that subjects' movement speed ranged between 150 and 250 deg/s, the peak torque applied to the arm was, on average, similar between the perturbation conditions. After these 160 trials, they completed another null block of 60 trials (null-2). Note that

the actual mapping between the handle (forearm) orientation and the cursor remained constant across the experiment. The only component that was perturbed was torque. The moment of inertia of the motor rotor was 9.3×10^{-5} kgm^2. The moment of inertia of the rod was 1.6×10^{-3} kgm^2 (weight: 2 kg; diameter: 4 cm). The rod was supported at each distal end by an Accrolon 9000 series nonmetallic self-lubricating sleeve bearing (Accro-Seal) and at its middle by a custom-designed plastic ball-bearing, making any friction minimal.

Randomly interspersed "NoGo" trials constituted 25% of each block. The motor was shut off on NoGo trials (i.e., it did not apply a force onto the subjects). Behavioral data, collected on Go and NoGo trials, confirmed that during NoGo trials subjects maintained a static orientation. We cannot exclude the possibility that subjects increased grip force in the NoGo trials, but this seems highly unlikely because the motor was shut off on these trials.

Behavioral measures

Custom-written software was used for graphics, data acquisition (LabVIEW 7; National Instruments, Austin, TX), and analysis (Matlab, The MathWorks, Natick, MA). Motion was sampled at 1,500 Hz using a 4,000-line optical encoder and low-pass Butterworth filtered (10-Hz cutoff) off-line. The movement "out" and movement "back" components were separated by the reversal position. The position data for each movement component were differentiated and movement onsets and offsets were defined. Movement onset for each component was defined as the time at which the velocity exceeded and remained >5% of the peak velocity for >100 ms. Movement offset for each component was defined as the time when the velocity fell and remained <5% of the peak velocity for >100 ms. Four dependent measures were analyzed (pooled across the four starting locations): *1*) absolute error, calculated as the absolute angular difference between the vectors $\overrightarrow{\text{CTr}}$ and $\overrightarrow{\text{CSr}}$ (reversal error) and between the vectors $\overrightarrow{\text{CTf}}$ and $\overrightarrow{\text{CSf}}$ (terminal error); *2*) variable error, calculated as the SD of error; and *3*) time to peak acceleration (TPA) within the first 12.5° of movement. This interval was chosen because it ensured that the positional field was not yet enabled and the viscous field was minimal. Thus TPA reflected anticipatory-based or very early control-based strategies. Data in each condition were fit with an exponential decay function defined by $y = a - b * e^{-t/c}$, where a is the magnitude of a dependent variable in the last trial, b is the difference between values in the first and last trials, c is the decay constant that represents the number of trials required to attain a roughly 63.2% improvement in performance, and t is the trial number. The decay constant (c) was used as a measure of learning rate (Martin et al. 1996). Error and TPA were analyzed using two-way ANOVA with factors: learning (early, late [mean of the first and last five trials, respectively]) and perturbation (null-1, null-2, positional, viscous). Learning rate was analyzed with a one-way ANOVA with perturbation as a factor. The Student–Newman–Keuls test was used for post hoc analysis. Significance was set at $P < 0.05$.

Magnetic resonance imaging (MRI) protocol

Imaging was performed using a 1.5-T GE scanner with a standard birdcage head coil. Three fMRI runs, each containing 332 functional volumes were obtained (*Run 1*: trials 1–60 null-1 and trials 61–93 torque-field; *Run 2*: trials 1–93 torque-field; *Run 3*: trials 1–34 torque-field and trials 35–94 null-2). Transitioning between the null and the torque-field conditions within a run ensured that any differences in performance would be directly attributed to the task rather than to any block-to-block effects. The first four functional volumes from each run were discarded to allow longitudinal magnetization to reach equilibrium. The functional runs were collected with: gradient-recalled echoplanar imaging, sensitive to BOLD contrast; TR, 2,500 ms; TE, 35 ms; flip angle, 90°; field of view, 24; 26 slices with a thickness of 3.5 mm and a 1-mm gap; on a GE Signa Horizon LX 1.5 T scanner. Anatomical images collected include: coplanar T1-weighted and a high-resolution image using the SPGR sequence for use in spatial normalization.

Device shielding

Radiofrequency and electromagnetic interference between the electric motor and the scanner were minimized by several means (Chinzei 1999). *1*) The motor was housed in specially constructed copper and MUMETAL nesting boxes (Magnetic Shield, Bensenville, IL). *2*) The nesting box housing the torque motor was placed as far as possible away from isocenter, within the 1- to 3-Gauss range (zone 4 according to Chinzei 1999). *3*) The computer (NI-PXI 8176), digital servoamplifier (Accelus ASP-180-18, Copley Controls), and power supply (PST-070-08-DP-E, Copley Controls) were placed outside the scanner suite (in the technician room). *4*) All wires connecting the controllers to the motor were twisted-pair cables and triply shielded using the wires' own shielding as well as copper mesh and MUMETAL hoses. *5*) All shielding materials were earth-grounded. We verified that any device-induced interference into the functional imaging data was negligible by testing individuals ($n = 3$) under three task conditions as they prosupinated their forearm at a self-paced 1 Hz: *1*) with the motor on applying a positive viscous torque as described above, *2*) with the motor unplugged, *3*) and with the motor out of the room. In each condition, subjects alternated between 20 s of movement and 20 s of rest for three cycles (TR = 2.5 s, 24 functional volumes per movement condition per subject). The imaging data were processed as described above. Qualitatively, no changes in image quality were evident in the functional volumes as a function of whether the motor had current passing through and delivered a torque or was unplugged or was entirely out of the scanning suite. This is illustrated in Fig. 2 (*bottom right* image in the three panels) by a sample axial slice taken from a randomly selected functional volume of one of the subject's movement conditions. To quantify this, a region of interest (ROI) was defined by a box ($1 \times 1 \times 1$ cm) in the left motor cortex based on a movement > rest contrast (Fig. 2, three panels). A signal-to-noise ratio (SNR, mean/variance) was computed within the ROIs for the

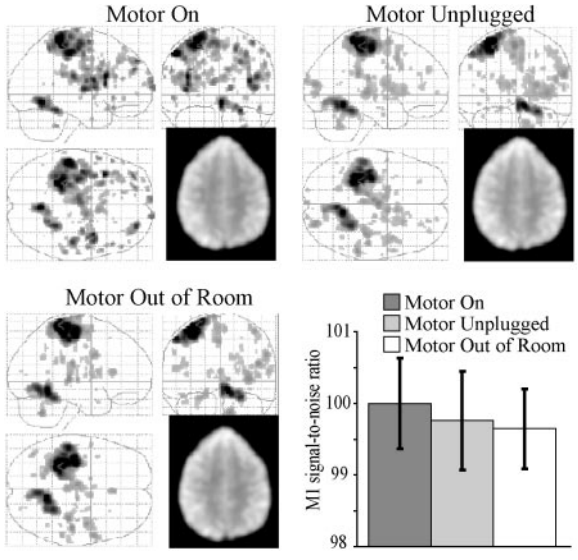

FIG. 2. Mean activations for a representative subject in 3 conditions: motor on (*top left*), motor unplugged (*top right*), and motor out of the room (*bottom left*). A sample axial slice through a randomly selected functional volume is shown for each panel. *Bottom right*: mean group signal-to-noise ratio in each condition for a $1 \times 1 \times 1$-cm region of interest (ROI) in the left motor cortex. No significant difference was noted as a function of whether the motor was on, unplugged, or not present in the scanning suite.

second through the next-to-last functional volume of each movement-related miniblock (total, 18 volumes per condition). The SNR for each condition is plotted in Fig. 2, *bottom right*. Preplanned unpaired *t*-tests between each condition revealed no significant changes in the SNR across the three conditions (Torque vs. Unplugged: $t(34) = 1.09$, $P = 0.29$; Out of room vs. Torque: $t(34) = -1.78$, $P = 0.08$; Out of room vs. Unplugged: $t(34) = -0.55$, $P = 0.59$). These results, as well as qualitative observations, strongly suggest that any possible interference is likely to be a negligible confound to the imaging data.

MRI data preprocessing and statistical analysis

The functional imaging data were analyzed with Statistical Parametric Mapping (SPM2; Wellcome Department of Cognitive Neurology, London, UK). Motion correction was performed for each subject to the first functional volume, using a six-parameter rigid-body transformation, and a mean of the corrected images was created. The mean functional image was coregistered to the subject's coplanar T1-weighted image and subsequently coregistered to the subject's high-resolution SPGR anatomical image, using mutual-information coregistration to the high-resolution anatomical scan. The high-resolution anatomical scan was spatially normalized to the Montreal Neurologic Institute template (Talairach and Tournoux 1988) by applying a 12-parameter affine transformation and a nonlinear warping with basis functions. Combined transformation matrices were applied to the functional images. The spatially normalized functional images were smoothed using a 6-mm Gaussian kernel.

Condition-specific differences in the BOLD signal were analyzed with a general linear model approach for event-related fMRI using SPM2. A design matrix with vectors for null (combined null-1 and null-2), positional, and viscous conditions for "NoGo" and "Go" trials was created individually for each of the 15 subjects. Null-1 and null-2 were concatenated into a single column in the design matrix (one column for Go and one column for NoGo trials). This was done because we had no a priori hypotheses regarding differences between these two conditions and no significant behavioral differences were noted. However, combining the two together considerably increased the statistical power of the baseline condition in the imaging analysis. In subtraction methods for imaging analysis, having a robust baseline condition is invaluable and often neglected. Run-to-run regressors were included in the design matrix to account for any nonspecific run-to-run effects. The onset and duration of each event, obtained from time stamps recorded during the experiment, were entered into the model and convolved with the canonical hemodynamic response function (HRF). Between-condition differences in BOLD magnitude were estimated for: *a*) all "Go" conditions > rest, *b*) all "NoGo" conditions > rest, *c*) positional-null > viscous-null, and *d*) viscous-null > positional-null (contrasts *c* and *d* were generated separately for "NoGo" and "Go" trials). The null condition was subtracted out in *c* and *d*, resulting in contrasts reflecting only adaptation to perturbations. Note that the NoGo trials in the null condition did not carry the same conditional aspect of motor planning that the perturbation trials had. Therefore subtraction of the null condition from the perturbation conditions ensured that these contrasts would reflect choice planning to each perturbation rather than sensorimotor transformations that remained constant across all conditions and that were not a focus of this investigation. Conversely, in the torque-field conditions, movement preparation was equally required in "Go" and "NoGo" trials, but movement implementation was unique to "Go" trials. Thus activation in the "NoGo" trials represents preparation, whereas that in "Go" trials represents preparation + implementation.

Contrast images were then passed on for random effects analysis at the group level. In addition to between-task contrasts, we correlated performance error with the corresponding magnitude of the BOLD response on a trial-by-trial basis, modeled together for the three perturbation conditions. A threshold magnitude of $P < 0.001$ (uncorrected) and extent of 10 voxels was used for all imaging analysis.

BOLD coherence

In addition to the traditional BOLD subtraction approach, we were interested in understanding whether functional interactions between distributed neural regions change as a function of learning, adaptive strategies, and processing stages (plan retrieval vs. execution). To address this, we enlisted a long-used approach in neurophysiology—one that has recently been applied to neuroimaging—that involves analysis of the coherence of the BOLD signal between regions of interest (ROIs that we identified from contrasts *a* and *b*). Coherence, unlike correlation, singly accounts for signal magnitude and timing, without the complication of interpreting temporal phase lags inherent in cross-correlation methods. Furthermore, coherence-based analysis allows for direct interpretation of functional interactions, which can be assumed only from traditional contrasts (Curtis et al. 2005; Miller et al. 2005; Sun et al. 2004). Finally, event-related coherence is more robust than block-averaging in characterizing learning-dependent changes because coherence captures trial-to-trial neural dynamics that are otherwise obscured by within-block averaging.

Coherence was calculated using Matlab according to the protocol described by D'Esposito and colleagues (Sun et al. 2004), where coherence (Coh_{xy}) is the coherence between the event-related time series of two given voxels (x and y); $f_{xy}(\lambda)$ is the cross-spectrum of x and y; and $f_{xx}(\lambda)$ and $f_{yy}(\lambda)$ represent the power spectrum of x and y, respectively, at frequency λ (*Eq. 1*). Typically, coherence among neural circuits is dependent on two factors: the bandwidth of the HRF (0–0.15 Hz; Aguirre et al. 1997) and the frequency of the events (in our case, about 0.125 Hz). We therefore chose to analyze coherence within this bandwidth. However, to tailor the bandwidth more precisely to our task while accounting for any slight fluctuations in trial-to-trial event frequency, we computed the mean coherence within a slightly narrower bandwidth (0.1–0.15 Hz). Our choice for this bandwidth is also consistent with data from a previous investigation of coherence at low- and high-frequency bandwidths (Sun et al. 2004). This study found that a low-frequency bandwidth (0–0.2 Hz) is sensitive to coherence between distributed regions, whereas a high-frequency bandwidth (0.2–0.4 Hz) is more sensitive to coherence between spatially adjacent voxels (Sun et al. 2004). Because we were interested in functional interaction between distributed regions, choosing a higher bandwidth would not be appropriate

$$Coh_{xy}(\lambda) = \frac{|f_{xy}(\lambda)|^2}{f_{xx}(\lambda) f_{yy}(\lambda)} \quad (1)$$

We generated condition-dependent time series for each voxel of interest by concatenating the convolved, event-related HRF for similar trial types into a single waveform. Every single event (60 "Go" and 20 "NoGo" trials in the viscous and 60 "Go" and 20 "NoGo" trials in the positional condition) were included. After this, the waveforms were mean centered and each subject's null condition time series was subtracted from his/her torque-field condition time series, for planning and execution epochs. The intent of this subtraction was to subtract out temporal dynamics not exclusively related to adaptation to the torque fields. To analyze learning-dependent changes, the first third and final third of each voxel's resultant waveform, for each condition, were extracted and used in the coherence analysis. The middle third was omitted to keep the early–late learning analysis of the imaging data consistent with the early–late analysis of the behavioral data. Note that an unavoidable consequence of concatenating event-related epochs is that coherence comes to represent event time rather than real time (as would be the case in a blocked design). This issue was also faced by Sun et al. (2004), although their individual events were longer than ours.

To generate a set of regions for entry into the coherence analysis we selected classic brain regions known to be involved in sensorimotor control from among those activated in the "Go" > rest (contrast *a*) and "NoGo" > rest (contrast *b*) contrasts (see Fig. S1). Two subcortical regions were also added: the left posterior putamen, which was

significantly activated in the viscous > positional contrast, and the right dentate. This is justified given the known involvement of these nuclei in motor control. The set of 20 regions is itemized in Table 2. The coherence analysis was performed on a subject-by-subject basis, thus generating 15 coherence values (one per subject) for each pairing of the 20 ROIs, each perturbation condition (positional and viscous), each trial type ("NoGo" and "Go" trials), and for each learning stage (early and late thirds).

Analysis of BOLD coherence

This procedure involves three steps and each step is illustrated in Fig. 3 using a small hypothetical data set. The first step involves organizing the data into a symmetric matrix wherein each cell of the matrix represents the coherence magnitude between imaginary regions *a*, *b*, *c*, *d*, and *e*. In Fig. 3 (step 1) each cell is color coded to the magnitude of the coherence value (blue to red corresponding to 0–1 range), with the value also printed into each cell. Note that the diagonal is all ones, indicating that each region is perfectly coherent with itself. We then averaged together all of the symmetric 20 × 20 matrices of coherence values for the 15 subjects to generate a group mean coherence matrix. This was done separately for each task and training period.

The second step was to identify condition-specific differences in coherence within the set of 20 regions using a nearest-neighbor linkage analysis in Matlab. The goal of the linkage analysis is to organize all of these pairwise interactions based on the relative difference in the strength of each pair of coherence measurements. Note that these are relative differences in pairs of coherence values, not differences between voxel locations. Operationally, this is done by first measuring the normalized differences between coherence values using the Euclidean distance, which is generally computed by finding the square of the distance between each variable, summing the squares, and finding the square root of that sum. In our implementation it was calculated with the Matlab function pdist.m within the statistics toolbox (using the nearest-neighbor method), where the input is the symmetric 20 × 20 matrix of average coherence values. Use of the nearest-neighbor method minimizes the probability that clusters would be artificially created (Rencher 2002). Note that the distances were calculated across the rows in the matrix, so the distances for any two coherence pairs become normalized to all other pairwise observations. In Fig. 3*A*, when the example matrix is evaluated with the pdist.m function the result is Fig. 3*B*. This set of pairwise distances is then passed through the Matlab function linkage.m to create a heirarchical cluster tree that is plotted as a dendrogram using the Matlab function dendrogram.m. In the dendrogram (Fig. 3, step 3) the linkage, or dissimilarity score, is plotted along the *x*-axis and the regions plotted along the *y*-axis. Smaller scores represent stronger linkages (or less dissimilarity). Thresholding this score (i.e., vertical line at 0.9 in this figure) allows one to cluster pairings into common families. Thus Fig. 3 (step 3) illustrates that regions *c*, *e*, and *d* are more tightly linked to each other (and form a common cluster shown in red) than *a* and *b*, but that *b* is more similar to this cluster than is *a*. The dendrogram provides an objective method for determining whether the overall pattern of values within the coherence matrix, across the 20 regions, changes as a function of task or learning.

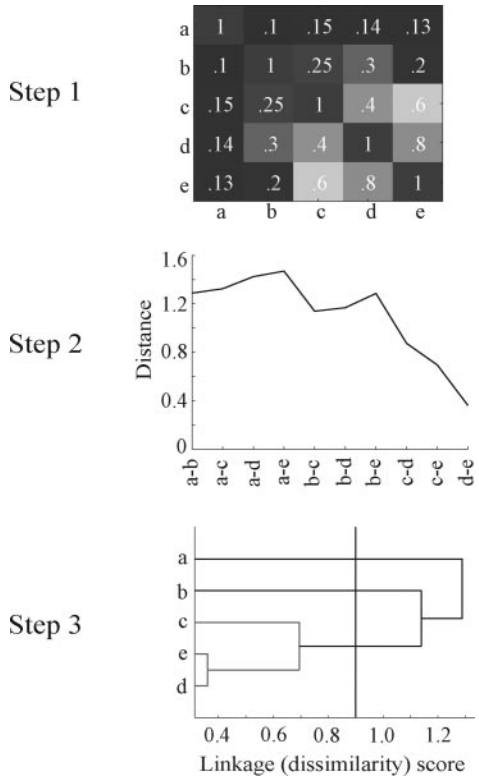

FIG. 3. Description of the linkage analysis used to interpret the coherence data. See corresponding text in METHODS for a detailed description.

We were most interested in identifying functional interactions between three major distributed systems: cortical, basal ganglia, and cerebellar. Thus we determined the lowest possible threshold (1.04) that would consistently yield between two and four clusters in all of the late-learning coherence analyses. This threshold was then used for viewing the dendrograms of all conditions. Statistical analysis of cluster solutions is not trivial because of the high dimensionality of the data [(19 × 20)/2 = 190 possible comparisons in each condition]. Multiple comparisons therefore are a suboptimal approach for quantifying differences between conditions (Rencher 2002). Instead, cluster validation is a recommended approach (Rencher 2002) wherein the validity of each cluster is substantiated. Validation of the cluster solutions was performed according to Rencher (2002) by randomly assigning each of the 15 subjects to one of two groups (group A and group B). A linkage analysis was then performed for the 20 voxels of interest on the entire functional time series in real-time (i.e., collapsed across all conditions) for groups A and B. Validity should be reflected as a consistent assignment of clusters for the A and B groups (see RESULTS). Note that this was strictly done for validation of the linkage procedure and not for interpretation of the data.

RESULTS

Behavioral data

Our intent was to train subjects to adapt to two different perturbations. After completing the experiment, each participant reported that the two perturbations were clearly distinct from one another. When asked whether they assumed a particular strategy for either torque-field condition, a typical response for the viscous perturbation was: "I just moved my arm more forcefully to get to the target." Conversely, a typical response for the positional perturbation was: "I had to control my arm from going past the target." Analysis of movement kinematics supported such subjective remarks. Figure 1*B* shows a representative participant's outward trajectories in the presence of a null perturbation (thick black line), positional perturbation (*left*), and viscous perturbation (*right*). A significant *perturbation condition* main effect for absolute error (Fig. 2, *inset*) [$F(3,42) = 27.3$, $P < 0.0001$, mean squared error (MSE) = 21.8] suggested that of the two, the positional perturbation was more disruptive. Additionally, the number of trials required to attain roughly 63.2% improvement in performance (learning rate) was considerably greater for both torque

perturbations relative to the null condition (Fig. 4) (null-1 and null-2: nine trials; viscous: 13 trials; positional: 25 trials). This difference, however, did not reach significance [$F(3,42) = 2.1$, $P = 0.12$, MSA = 389].

In spite of these between-perturbation differences and the random practice schedule, subjects nevertheless showed evidence of adaptation. First, a significant reduction in absolute error was noted from the early to the late trials (Fig. 4) [viscous, 56.9%; positional, 36.8%; learning stage main effect: $F(1,14) = 48.9$, $P < 0.0001$, MSE = 17.1]. Second, a significant reduction in variable error was noted from the early to the late trials [viscous, 61%; positional, 53.7%; $F(1,14) = 11.8$, $P < 0.01$, MSE = 268.3]. Significant *perturbation condition* × *learning stage* interactions for absolute error [$F(3,42) = 11$, $P < 0.0001$, MSE = 15.4], variable error [$F(3,42) = 11$, $P < 0.0001$, MSE = 122.6], and post hoc analysis revealed that these gains were greater in the viscous condition. Third, subjects showed evidence of recalling field-specific adaptive strategies based on the provided contextual cue. This was evidenced by a significant *perturbation condition* main effect [$F(3,42) = 53.5$, $P < 0.0001$, MSE = 164] and *perturbation condition* × *learning stage* interaction for TPA [$F(3,42) = 3.2$, $P = 0.03$, MSE = 142] (Fig. 5). Post hoc analysis for TPA revealed that by late learning, subjects took 8.8% longer to reach TPA in the positional condition but 21.1% shorter to reach TPA in the viscous condition. Note that TPA was measured within the first 12.5° of movement onset (i.e., before the onset of the positional perturbation and when the viscous perturbation was minimal), ensuring that differences in TPA were unlikely accounted for by perturbation effects.

To ensure that subjects indeed learned two distinct motor control policies, each unique to a perturbation, we tested an additional group of subjects ($n = 5$) out of the scanner on a slightly modified version of this task. In this experiment, subjects encountered a null perturbation (catch trial) on 10% randomly presented trials that were embedded within the torque-field block. For catch trials, subjects were still presented with the color-coded target (red for viscous and blue for positional), although the perturbation never occurred during

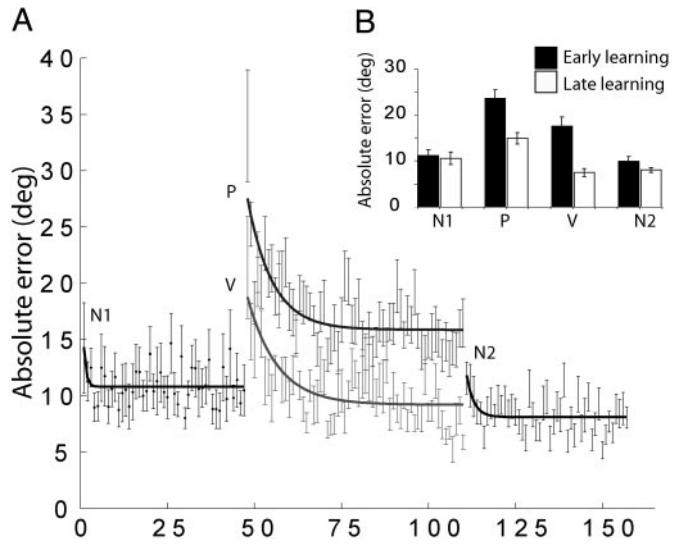

FIG. 4. Mean group absolute error ± SE, fitted with an exponential decay function. *Inset*: mean error for the 1st and last 5 trials: null (N1 and N2), positional (P), viscous (V).

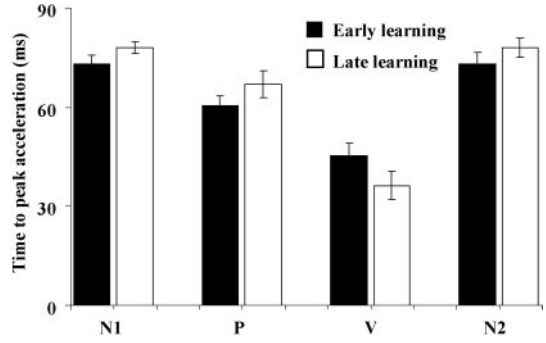

FIG. 5. Group mean (±SE) for time to peak acceleration (TPA) for the 1st and last 5 trials in the null (N1 and N2), positional (P), and viscous (V) conditions.

the movement. We hypothesized that if subjects learned distinct motor-execution strategies, then aftereffects should be observed on the catch trials and these aftereffects should differ between the two perturbation conditions. Alternatively, if subjects utilized a common control strategy for both perturbations (i.e., by stiffening their arm regardless of perturbation type), then aftereffects would not be evident or not differ between the two perturbation conditions. Figure 6*A* shows randomly chosen trajectory profiles of one participant's outward movements in the positional and viscous conditions (solid lines) and for their respective catch trials (dashed lines). Qualitative inspection of

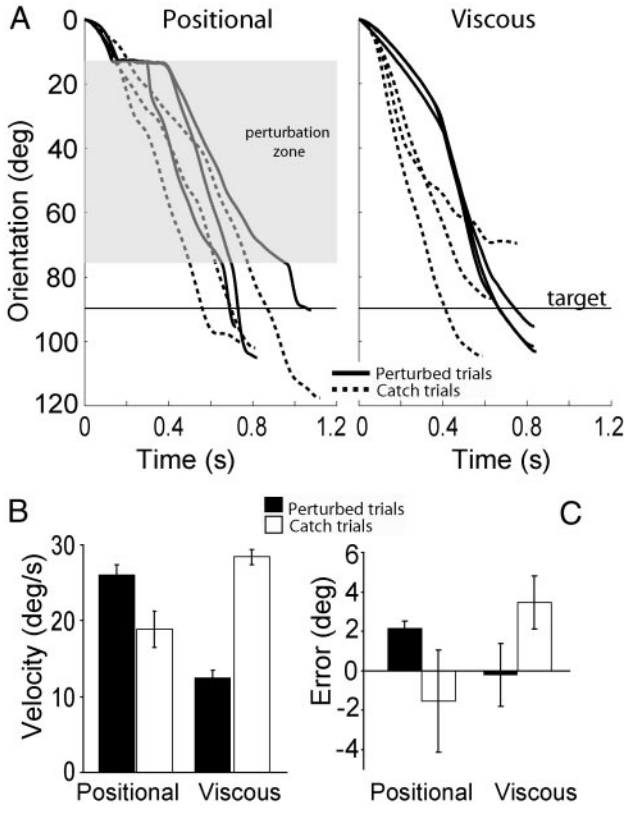

FIG. 6. *A*: last 3 trajectory profiles of one subject's outward movements during an actual perturbation trial type (solid lines) and an unexpectedly presented null field (catch trials) (dashed lines). For catch trials, subjects were provided with either the viscous or the positional contextual cue, but never actually received the perturbation during the movement. Mean group (*B*) peak angular velocity within the first 17° of the movement and (*C*) signed error, both showing significant aftereffects in the catch trials for each perturbation condition.

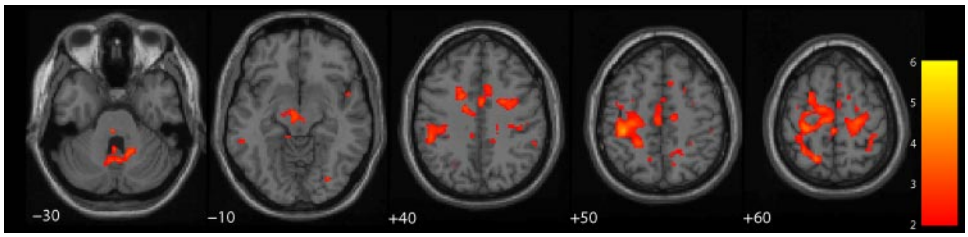

FIG. 7. Regions showing a positive correlation between blood oxygenation level–dependent (BOLD) activation and error magnitude (threshold, $P < 0.01$; extent, 10 voxels). Image left is the left hemisphere.

the trajectory profiles shows clearly that aftereffects were not only evident, but also differed between the two perturbation conditions (note the slope in the early portion of the movement). To quantify any such differences, we analyzed two dependent measures: the peak angular velocity within the first 17° of movement (this time interval extended just beyond the occurrence of the perturbation, ensuring that the aftereffect would be captured by this measure) and signed error [calculated as the angular difference between vectors $\overrightarrow{CTr}$ and $\overrightarrow{CSr}$ (for reversal error) and between vectors $\overrightarrow{CTf}$ and $\overrightarrow{CSf}$ (for terminal error)]. Group data for each variable were analyzed using a repeated-measures ANOVA with factors perturbation type (positional, viscous) and trial type (torque, catch). Torque trial types contained the mean of the last 10 torque-field trials to ensure that these data represented well-learned motor behaviors and catch trial types contained the mean of the final two catch trials. A significant main effect of trial type (torque, catch) was noted for peak angular velocity [$F(1,4) = 18.5$, $P = 0.01$], confirming a general occurrence of aftereffects in both conditions. A significant torque-field (positional, viscous) × trial type (torque, catch) interaction was also noted [$F(1,4) = 123.1$, $P < 0.001$] (Fig. 6*B*), indicating that aftereffects differed between the two catch trial types. Post hoc testing revealed a significant difference between each torque condition and the respective catch trial as well as between the two catch trial types. We also analyzed signed error. A significant torque-field (positional, viscous) × trial type (torque, catch) was for signed error [$F(1,4) = 10.2$, $P = 0.03$] (Fig. 6*C*). Post hoc analysis again revealed significant differences between each torque-field condition and its respective catch trial, as well as between the two catch trial types. These results strongly suggest that subjects used two different motor control policies—each specific to the distinct perturbations. Given this, we proceeded to analyze the imaging data to understand the corresponding neural processes.

TABLE 1. *Regions showing significantly greater brain activation for movement execution in the viscous than the positional field, with null field subtracted from both conditions*

			Viscous > Position				
		Side	T	Z	*x*	*y*	*z*
Putamen	Ventral-posterior	R	6.54	4.36	27	−3	−9
	Ventral-anterior	R	5.81	4.08	21	18	−3
		R	4.60	3.53	21	12	−12
	Posterior	L	6.30	4.27	−33	−9	−3
	Anterior	L	6.04	4.17	−21	3	−3
	Anterior-superior	L	5.34	3.88	−21	6	12
Caudate	Head	R	5.66	4.02	24	27	6
		L	6.75	4.43	−3	−60	24
Frontal	SMA	L	4.38	3.42	−3	−12	66
	Subcallosal g.	L	5.18	3.81	−18	15	−18
Cingulate	Anterior g.	R	5.67	4.02	3	60	3
		L	4.87	3.67	−9	57	−3
	Posterior g.	R	8.18	4.88	6	−48	15

Activation threshold and extent set at $P < 0.001$ and 10 voxels, respectively. The reverse contrast, positional-null > viscous-null, did not yield any significant activations even at a more liberal threshold of $P < 0.01$.

Correlation between brain activation and performance

To test for direct relationships between performance and brain activity, each subject's error magnitude was correlated with the BOLD magnitude, collapsed across the null, viscous, and positional perturbation conditions (all "Go" trials). Figure 7 shows that activity in three regions was positively correlated with performance error: the right dentate nucleus (*x*, *y*, *z* of local maxima: 15, −51, −30), the left intraparietal sulcus (−30, −51, 54), and the left sensorimotor cortex (−27, −27, 57). In other words, as trial-to-trial error was reduced, activity within these regions also decreased, implicating their involvement in general trial-to-trial learning on our task.

Brain activation for different adaptive responses

Subjects first trained in the null condition, wherein they encountered only minimal frictional resistance. The BOLD signal for the "Go" and "NoGo" trials in the null perturbation condition was contrasted with rest to define those areas involved in such a visuomotor transformation (Fig. S1[1]). The "Go" > rest contrast yielded activation in cortical and subcortical motor circuits, including bilateral thalamus, bilateral anterior cerebellar cortex, bilateral posterior parietal cortex along the intraparietal sulcus, and the arm representation area of the left primary motor cortex. The "NoGo" > rest contrast yielded an activation pattern similar to that of the above contrast, but with reduced activation of the sensorimotor areas. The "NoGo" contrast additionally yielded activation of the left inferior frontal gyrus, pars triangularis, and pars opercularis that was not observed in the "Go" contrast.

After the null condition, subjects trained on the positional and viscous perturbations, each with an assigned contextual color cue. To define perturbation-specific activations, the positional and viscous conditions were contrasted against each other after subtracting out the null condition from each torque-field condition. This subtraction was intended to eliminate activations exclusively related to visuomotor transformations. It does not eliminate effects related to choosing among context-defined motor responses. The viscous-null > positional-null contrast for the "Go" trials yielded a relative increase in the bilateral putamen, caudate head, anterior cingulate gyrus, right posterior cingulate gyrus, and the left SMA (Table 1 and Fig. 8). The reverse, positional-null > viscous-null, contrast for

[1]The online version of this article contains supplemental material.)

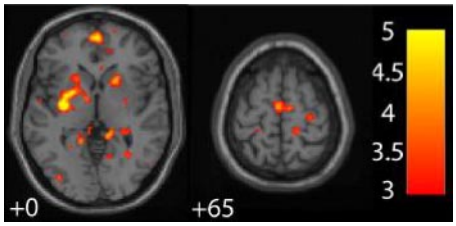

FIG. 8. T-map image of the viscous-null > positional-null contrast for movement implementation showing left SMA and putamen activation (threshold, $P < 0.001$; extent, 10 voxels). Reverse contrast for execution, as well as both contrasts for movement planning, yielded no activation at this threshold. Null condition has been subtracted from both contrasts to focus exclusively on regions involved in adaptive responses to the perturbations. Image on *left* is left hemisphere.

"Go" trials showed no significant activation at this threshold. These findings suggest a limited degree of additional neural recruitment for the execution of movements in a viscous relative to positional perturbation. Aside from this additional recruitment, analysis of BOLD magnitude suggested that adaptation to either perturbation was not only attributed to overlapping regions, but also that these regions were activated to a similar extent for each perturbation condition. Moreover, neither the viscous-null > positional-null nor the positional-null > viscous-null contrast for the "NoGo" trials showed any significant activation at that threshold, again suggesting that planning for the different adaptive responses was attributed to common anatomical regions activated to similar extents across the perturbation conditions.

Network coherence for different adaptive responses

BOLD coherence was analyzed to characterize functional neural interactions on a network level. All regions prescribed to this analysis are listed in Table 2. Of particular interest were interactions between cortical, cerebellar, and basal ganglia systems during *1*) the early and late learning stages, *2*) between each perturbation condition, and *3*) for the contextually cued preparation versus the movement execution epochs of each trial. Figure 9 shows the coherence matrices for each condition with the magnitude of coherence color-coded (warmer = stronger; colder = weaker). The ROIs are labeled along the *x*–*y* axes (see Table 2 for *x*–*y* label assignments). The values along the diagonal represent a perfect coherence between a given region and itself (value of 1). The matrices were re-sorted to optimize visualization of the data. Re-sorting was performed by associating each matrix with a Laplacian matrix and then sorting the components of a specified eigenvector of the Laplacian (Barnard et al. 1995; Johansen-Berg et al. 2004). The late-learning viscous condition matrix was chosen as the canonical matrix and all other matrices were re-sorted to this ordering. Note the matrices are not symmetrical because movement preparation and execution conditions have been assigned to the top and bottom triangles of the matrix, respectively.

Qualitative evaluation of Fig. 9 reveals that coherence increases for some regional pairings and decreases for others from the early (*left column*) to the late (*right column*) learning stage. For example, by late learning in the Go trials of the

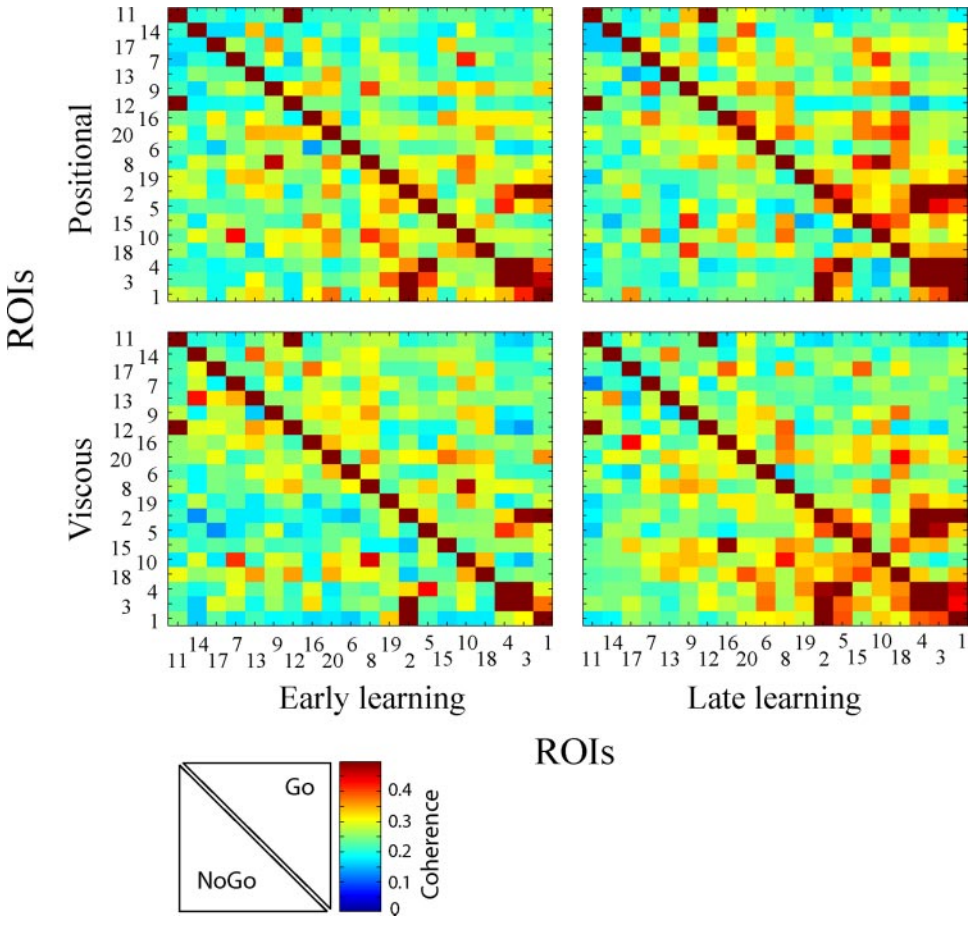

FIG. 9. Coherence matrices for contextually cued recall (bottom triangle) and movement implementation (top triangle) are shown for positional (*left*) and viscous (*right*) conditions during early (*top*) and late (*bottom*) learning. *x*–*y* axes correspond to the ROI number codes in Table 2. Coherence magnitude is color scale-coded (hot:strong, cold:weak). Values along the diagonal are equal to one. Note that all of the matrices have been sorted (see METHODS) according to the viscous, late learning, condition for clarity: *x*–*y* labels of the ROIs are thus numbered accordingly.

TABLE 2. *Regions of interest (ROIs) selected for coherence analysis*

ROI Name	*x*	*y*	*z*
1. Putamen1*	−24	9	6
2. Putamen2*	−24	6	6
3. Putamen3*	−25	0	6
4. Putamen4*	−25	−3	6
5. Putamen5*	−25	−9	6
6. SMA	−9	−1	70
7. SMA1	−12	−27	66
8. SMA2	−3	−21	63
9. SMA3	−3	−12	66
10. SMA4	−3	−30	66
11. SMA5	−5	−30	75
12. SMA6	−3	−21	75
13. Dentate1*	18	−51	−33
14. Dentate2*	18	−42	−33
15. aIPS	−27	−54	39
16. mIPS	−33	−60	48
17. cIPS	−21	−69	36
18. PMd	−36	−9	54
19. PMv-operc.	−57	9	3
20. MI	−30	−33	60

Numbers on the left correspond to the *x*–*y* axis labels in Fig. 10. Asterisks denote regions that were not significantly activated in the "Go" > rest and "NoGo" > rest contrast.

viscous condition, coherence tends to increase between the putamen and ventral and dorsal premotor areas (PMv, PMd), the supplementary motor area (SMA), and the anterior intraparietal sulcus (aIPS) but tends to decrease between the dentate nucleus and the SMA, the aIPS and mIPS, the primary motor cortex, as well as PMv and PMd. Conversely, in the positional condition, coherence tends to increase between the dentate nucleus and SMA and the primary motor cortex but decreases between the putamen and the SMA. To quantify and validate such patterns in coherence, the coherence matrices for each trial type ("Go", "NoGo"), perturbation condition (positional, viscous), and learning stage (early, late) were submitted to a linkage analysis (see METHODS for details).

Linkage analysis computes the relative proximity of each voxel-pair permutation. This proximity measure can be clustered into families sharing similar values and the hierarchical organization of this clustering can be analyzed and visualized as a dendrogram (Fig. 10; see METHODS for details). Figure 10 shows the dendrograms for each condition, the *x*-axis representing the measure of proximity between each pairing listed on the *y*-axis. Because linkage computes the distance between the permutations, smaller values along the *x*-axis represent stronger linkages between the respective regions and larger values represent weaker links between regions. A threshold of 1.04 (see METHODS) was used as a quantitative method of reducing the multidimensional data set into clusters (dashed vertical lines in Fig. 10). This threshold operates much like a *P* value in descriptive statistics in the sense that linkages falling below this threshold are automatically classified into a common family (shown as gray regions in Fig. 10). It thus follows that the strength of coherence is greater *within* compared with *between* clusters.

Results of the linkage analysis support the qualitative trends noted in evaluating the coherence matrices shown in Fig. 9. Figure 10 illustrates that during the early learning stage, there was negligible specificity in interregional coherence. This was the case in the "Go" trials (Fig. 10*A*) and in the "NoGo" trials (Fig. 10*B*) trials of the viscous as well as the positional conditions and is reflected in Fig. 10 (*left column*) by the numerous separate clusters formed by cortical, basal ganglia, and cerebellar regions.

The linkage results for the late learning stage in the "Go" trials were characterized by a relative increase in coherence between a premotor–parietal-–putamen network in the viscous condition (Fig. 10*A*, *bottom right*) and a premotor–parietal–cerebellar network in the positional condition (Fig. 10*A*, *top right*). The black outlines depict the grouping of the largest clusters that contributed to this pattern. Note that this does not imply a noninvolvement of the cerebellum in the viscous condition or a basal ganglia noninvolvement in the positional condition. It is clearly evident that the cerebellum eventually links up with the main family in the viscous condition, although at a more distant linkage score (and the same for the basal ganglia in the positional condition). What this implies is that a common distributed network was involved in both perturbation conditions, although the functional interactions within this common network may have subtly varied as a function of the perturbation condition.

By late learning, the number of clusters was largely reduced. In the "NoGo" trials (Fig. 10*B*, *right*), two large families distinctly formed (black outline): a frontoparietal cortical cluster and a basal ganglia cluster. Although these were separate clusters, they were more strongly linked to each other than either one with the cerebellum.

The validity of the clustering method was verified by comparing the rank order of all of the ROIs, across all events for two groups of subjects (see Rencher 2002 and METHODS). The result of this analysis is shown in Fig. 11. The overwhelming similarity in the rank order of the brain sites and their respective linkages in the dendrograms ensures that this method was valid in prescribing clusters (see also Rencher 2002).

DISCUSSION

Adaptive strategies

Subjects trained on two very distinct torque perturbations in a randomly interleaved order. Before each trial, subjects were provided with a color-coded guide uniquely linked to each perturbation. In debriefing after the experiment, subjects reported that they readily learned to associate each color with the respective perturbation. The significant reduction in performance error confirmed that individuals learned to adapt in spite of training on a random practice schedule. This was not unexpected and it was previously demonstrated that humans are flexible in learning new skills in a variety of contexts—using arbitrary visual contextual cues to learn different randomly interleaved motor perturbations (Osu et al. 2004) or learning to modulate grasp aperture to perceived sound frequency (audiomotor mapping) (Safstrom and Edin 2006). A control experiment with catch trials included for each perturbation was designed to directly rule out the possibility that subjects deployed a universal cocontraction strategy for both perturbations. Peak angular velocity and signed error were both significantly larger in the catch trials than in the torque-field trials for

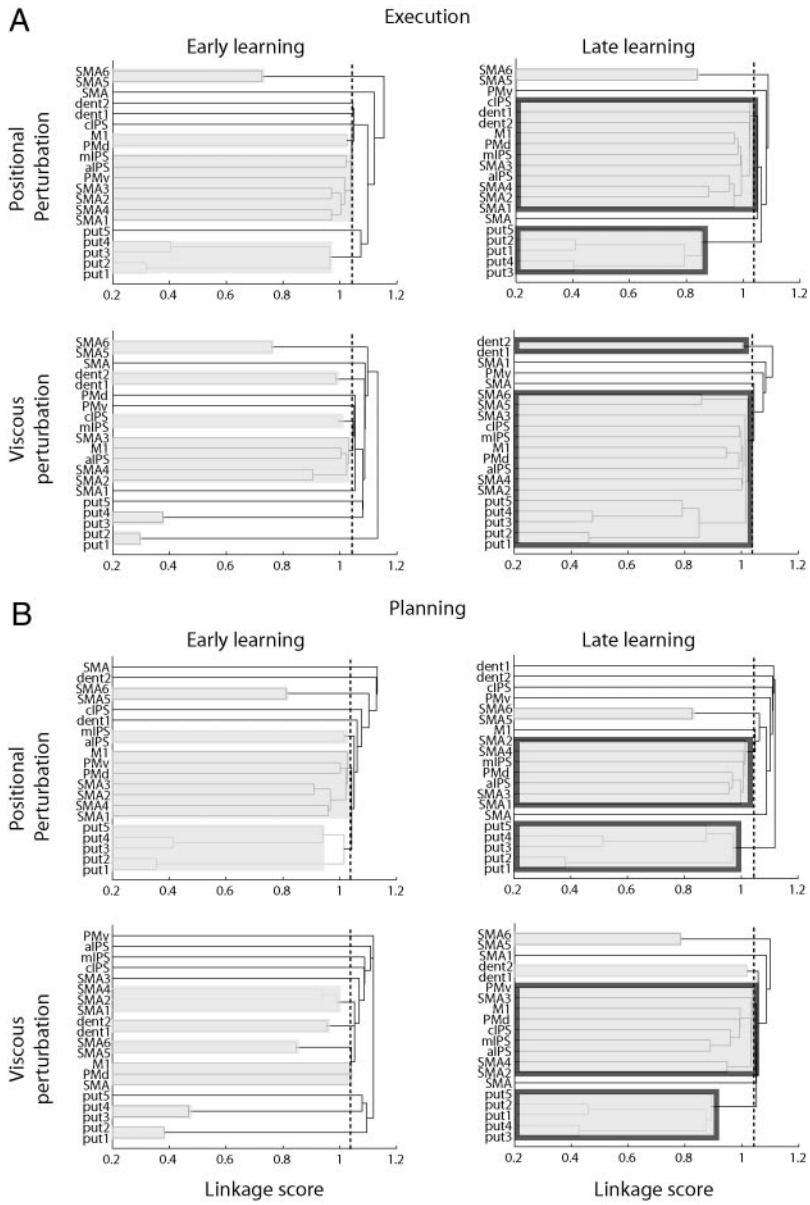

FIG. 10. Dendrograms of linkage analysis performed on the coherence matrix shown in Fig. 7 for movement implementation (*A*) and contextually cued recall (*B*). Note that the ordering of the ROIs (see also Table 2) shown on the *y*-axis is obligated to change for each condition because the hierarchical clustering of each pairing also changes as a function of condition. Dissimilarity score, computed by the linkage analysis, which determines the hierarchical order is shown along the *x*-axis. Gray boxes depict clusters formed using a 1.04 linkage score threshold (see METHODS). Note the late-learning formation of two distinct coherence patterns for movement implementation (*A*); between cortex and basal ganglia for the viscous condition and between cortex and cerebellum for the positional condition.

either perturbation condition, suggesting that at least to a considerable extent, subjects used field-specific strategies by the late learning stage. Empirical evidence supports this finding. For example, cocontraction strategies are predominantly observed only in the first few trials of learning and are generally deployed in cases of far more destabilizing perturbations than the types presented in our experiment (Milner and Franklin 2005). We subsequently discus the neural processes that may underlie the implementation of unique adaptive behaviors.

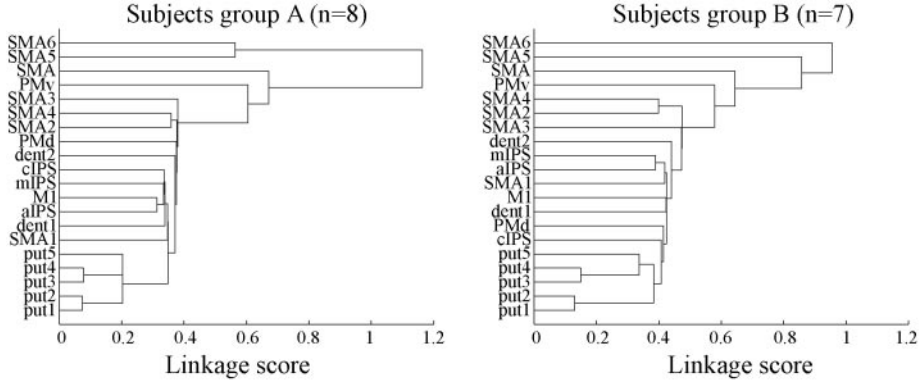

FIG. 11. Validation of the linkage analysis for 2 random samples (A and B) of the group. Note the consistency in the rankings of, and the linkages between, the ROI's shown on the *y*-axis for sample populations A and B.

Neural interactions underlying adaptation

Standard contrasts in our study revealed excess activation, particularly in the basal ganglia and the SMA, in the viscous-positional condition contrast but no excess activation in the reverse contrast. This excess activation was evident only in the "Go" trials and not observed for either contrast in the "NoGo" trials. If analysis ended here, one would conclude that for the most part, common circuits underlie adaptation under different dynamic conditions, although something may have been inherently different about the viscous condition that necessitated additional recruitment of the SMA and basal ganglia. Such a conclusion might even be corroborated by the findings of Diedrichsen et al. (2005), who investigated neural correlates of on-line adaptation for "kinematic" versus "dynamic" perturbations. In that study, Diedrichsen et al. (2005) noted few differences in activation, in their case between a "kinematic" and "dynamic" contrast. Both our initial analysis and that of Diedrichsen et al. (2005) make the assumption that BOLD magnitude alone is sufficient to unveil dynamic, task-specific, neural processes.

However, we also investigated an alternative explanation: that analysis of the temporal dynamics of neural interactions, which are not approachable through analysis of BOLD magnitude, may provide additional information. To this end, we analyzed the coherence of the BOLD signal in a distributed neural network involved in motor control and identified in the standard contrasts. Incorporating the temporal dynamics of the BOLD signal revealed perhaps it is not only the condition-specific difference in the intensity of activation across regions that governs on-line control, but also the functional interactions (coherence) between different regions. Thus coherence, which is more sensitive in detecting subtleties in functional neural interactions, may provide a robust means to identify functional interactions between distributed regions (Garraux et al. 2005; Sun et al. 2004). It was previously suggested that learning is associated with a gradual reduction in *within* cortical functional interaction and a gradual increase in *between* cortical–striatal interactions (Toni et al. 2002). Our results substantiate and extend this view by demonstrating that early learning was largely attributed to *within* cortical, basal ganglia, and cerebellar patterns. Conversely, late learning was characterized by differential functional neural interactions *between* these same anatomical regions; specifically a preferential interaction of a cerebrocortical–basal ganglia network for adapting to the viscous perturbation and a cerebrocortical–cerebellar network for adapting to the positional perturbation.

BOLD coherence and neural activity

Analytical methods for interpreting brain function using the BOLD signal have progressed considerably over the past decade. A potentially powerful approach recently applied to brain imaging is to compare the temporal changes of the BOLD signal between different brain regions. In other words, one can now ask: "How do regions interact with one another over time?"—rather than asking the traditional question: "Which regions have greater activity?" Analysis of coherence, long used in physiology, offers this window into understanding the functional interactions of neural circuits from MRI data (Curtis et al. 2005; Miller et al. 2005; Sun et al. 2004). Effectively, coherence is the normalized cross-correlation between two waveforms, but in spectral (frequency) space rather than in time. This property gives coherence to two important advantages over cross-correlation: no need to interpret positive and negative correlations that, given the complexity of the HRF, are often difficult to understand and, second, the ability to calculate coherence within the known frequency bandwidth of the HRF and the events, eliminating the need to account for time lags in correlation analysis.

Because of the event-related nature of our design, unavoidably the waveforms submitted to the coherence analysis are considered in "event" time rather than in real time (see also Sun et al. 2004). In other words, this analysis is capturing condition-specific systems level neuronal interactions. It is emphasized that making multiple comparisons [$(19 \times 20)/2 = 190$] per condition to isolate significant local interactions is not the purpose here nor is it the most valid approach (Rencher 2002). Instead, our intent was to understand systems-level patterns in interaction, how they change with task, processing stage, and learning. Linkage is the principled approach for defining such patterns of interactions in a multidimensional data set and in a fully reproducible way (Rencher 2002). The random sampling of the population confirmed the validity of this approach.

Given that the BOLD signal is thought to represent local field potentials, or local neural interactions (Attwell and Iadecola 2002; Logothetis 2003), it is of little surprise that the BOLD pattern was coherent among adjacent regions. In this regard, coherence may have been driven by both shared local field potentials and common functional interactions, possibilities that are difficult to dissociate. Conversely, coherence between spatially segregated regions, but those known to be mono- or polysynaptically connected (Clower et al. 2001, 2005; Eblen and Graybiel 1995; Strick et al. 1998), cannot be explained by simple epiphenomena such as spillover or enhancement of local field potentials among adjacent neural populations but rather reflect the active involvement of a distributed network in a common function.

This said, our results do not imply that cortical–basal ganglia networks always underlie adaptation to viscous perturbations and cerebellar–cortical networks to positional perturbations. Indeed if this were the case, it would be difficult to reconcile the breadth of findings from physiological recordings and imaging studies demonstrating that activity within cortical, cerebellar, and basal ganglia regions can correlate with various movement parameters, depending on the task (DeLong et al. 1984a,b; Fu et al. 1997; Messier and Kalaska 2000; Sergio and Kalaska 2003; Sergio et al. 2005; Turner et al. 2003). Such a redundancy within the sensorimotor system may instead underlie the nervous system's flexibility in preferentially choosing functional circuits that fit more global sensorimotor goals of the task.

Instead, we contend that the differential, perturbation-specific recruitment of common circuits was particularly attributed to the subjects' adaptation to the sensorimotor goals associated with each perturbation. The TPA results indeed suggest that subjects learned to initiate their movements in an increasingly optimal, perturbation-specific manner. Closer examination of the catch trial experiment data further indicates the presence of aftereffects in the early portion of the movement, which would not be expected if subjects did not develop and implement

perturbation-specific strategies or if subjects anticipated catch trials. Further evidence that catch trials, which were randomly interspersed (10%) throughout the perturbed trials, were not anticipated is the overlap in the perturbed and catch trial profiles before the trajectories entered the would-be perturbed zone (gray area, Fig. 6*A*, *left*) and, second, by the presence of aftereffects, which clearly would be absent if subjects anticipated catch trials.

A most probable explanation is that subjects learned to predict the angle at which the positional perturbation was engaged and disengaged (as they performed movements from different start positions and to different targets), but not the amplitude of the torque it exerted because the torque magnitude remained constant in this condition. Executing adaptive control in the positional perturbation condition led to a stronger coherence between cortical–cerebellar sensorimotor regions than cortico–basal ganglia regions. This finding is consistent with and supports an extensive literature-based linking of the cerebellum in the prediction of sensorimotor events (Blakemore and Sirigu 2003; Dreher and Grafman 2002; Miall et al. 1993; Nitschke et al. 2003; Nixon 2003; Timmann et al. 2000). In our study, this increased cerebellar–cortical coherence may likely be attributable to the increased effort in predicting the edges of the perturbation step.

Execution of this strategy, however, was unlikely to be appropriate for the viscous perturbation. For example, after repeated training in the viscous condition, subjects may have adapted a strategy wherein the braking of the movement, as it approached the target, could have theoretically been produced by the viscoelastic properties of the muscle rather than by the antagonistic muscles. This strategy has been shown to be used in situations when the agonist force is smaller than the passive viscoelastic tension of the ant(agonists) (Lestienne 1979), which may have been the case toward the end of the movement when the viscous torque was minimal. Clearly, however, this mechanism would not have been feasible in the positional condition, which required a substantial antagonist muscle burst to brake the motion. We thus contend that subjects adapted to the viscous perturbation by scaling their motor output. Indeed, subjects themselves reported that for this condition, they initially increased their force output to counteract the viscous resistance. Unlike in the positional perturbation, the viscous condition revealed a stronger basal ganglia–cortical coherence. The basal ganglia has been repeatedly implicated in scaling processes related to movement (Bergman et al. 1994; Desmurget et al. 2003, 2004; Georgopoulos et al. 1983; Turner et al. 2003; Vaillancourt et al. 2004; Wichmann et al. 1994a,b), which perhaps may also account for some of the hypometric deficits observed in Parkinson's disease.

In summary, we contend that the perturbation-specific motor control policies may have been guided by the engagement of neural circuits selected according to the sensorimotor goals that the subjects found most optimal in adapting to each perturbation.

Neural interactions underlying arbitrary visuomotor associations

We also investigated whether learning-dependent functional connectivity would exhibit specificity for contextually cued recall of adaptive responses to the two perturbations. Our findings suggested that contextual cues were successfully used to plan for the two oncoming perturbations, highlighting the importance of contextual cues in learning multiple adaptive strategies in a random practice schedule (Osu et al. 2004). Coherence was therefore analyzed in the "NoGo" trials to investigate whether contextually cued recall was attributed to the interaction among common or distinct neural circuits. Although no apparent interregional pattern in coherence was noted during early learning, a relative strengthening in the cortical and basal ganglia clusters was noted for both perturbation conditions during late learning. The involvement of these regions in contextually cued recall is in line with reports of increased activation in prefrontal, parietal, and basal ganglia territories in tasks that require the learning of arbitrary visuomotor associations (Boettiger and D'Esposito 2005; Toni and Passingham 1999; Toni et al. 2001) and movement preparation (Alexander and Crutcher 1990; Thoenissen et al. 2002). Importantly, Alexander and Crutcher (1990), who recorded cell activity in the arm representation neurons of the MC, SMA, and putamen while monkeys performed a step-tracking task, reported that the preparatory neuronal activity was perturbation nonspecific, suggesting that this network was engaged in a general plan selection process. This is consistent with other reports attributing the basal ganglia network in part to a role in building and selecting action plans (Gentilucci and Negrotti 1999; Jueptner and Weiller 1998; Kimura et al. 2003; Menon et al. 2000).

Performance and brain activity

Our behavioral data indicated that subjects learned to adapt to both perturbations and, remarkably, achieved this despite training in a random practice schedule. Adaptation was reflected by significant trial-to-trial improvement in absolute and variable error for each perturbation condition, although admittedly large differences in absolute error occurred between the viscous and positional conditions. To identify the neural regions exhibiting performance-related changes, we correlated the BOLD signal with absolute error, collapsed across tasks to avoid the confound of between-task differences in error. Reduction in overall performance error was associated with reduced activity in the left parietal cortex and the right dentate nucleus. This finding is not unexpected considering other imaging studies that similarly showed parietal and cerebellar regions to be modulated over the course of adaptation (Clower et al. 1996; Imamizu et al. 2000; Inoue et al. 1997, 2000; Miall and Jenkinson 2005; Nezafat et al. 2001). In particular, Nezafat et al. (2001) noted an initial reduction in rCBF to the dentate over the course of the first two scan sessions as subjects adapted to a novel torque perturbation. Although rCBF to the dentate increased in the following sessions, the number of trials performed during their first two sessions was almost equal to the number of perturbation trials performed in our study.

It may thus be that the parietal cortex and the cerebellum are implicated in aspects of on-line error detection/correction and use of such knowledge of results to update the motor plan on subsequent trials (trial-to-trial adaptation). Earlier lesion studies shed light on this conjecture. Parietal lesions, whether pathological or reversible as with TMS, largely disrupt on-line control of reaching and grasping in the face of various perturbations (Desmurget et al. 1999; Grea et al. 2002; Tunik et al. 2005) as well as trial-to-trial adaptation to perturbations (Della-

Maggiore et al. 2004). In this regard, we previously hypothesized that a partial role of the parietal cortex, and the anterior portion of the intraparietal sulcus, especially with respect to reach-to-grasp movements, may be to iteratively generate a difference vector throughout the evolving movement, what we referred to as a diagnostic error signal (Tunik et al. 2005), between the intended action goal and the current state of the system derived from sensory input. This information may then be used by the cerebellum to better predict or update the motor plan on subsequent trials, thus leading to trial-to-trial adaptation (Desmurget and Grafton 2000). Although this thesis has yet to be directly tested, it is further substantiated by imaging data showing adaptation-dependent modulation of the cerebellum in visuomotor learning paradigms (Graydon et al. 2005; Miall and Jenkinson 2005) and by observations that trial-to-trial adaptation is largely disrupted in patients with cerebellar lesions (Diedrichsen et al. 2005; Martin et al. 1996; Smith and Shadmehr 2005).

Strengths and limitations of the current findings

One potential limitation is that the notable difference in performance error between the two perturbation conditions may underlie the condition-specific differences in coherence patterns. This possibility is unlikely because the condition-dependent differences in error remained constant from the early to the late learning phases, whereas the coherence pattern showed an interaction between learning phase and perturbation condition. Second, the interpretation of a seemingly large number of conditions (perturbation [viscous, positional], trial type ["Go", "NoGo"], and learning phase [early, late]) may likewise be seen as a potential limitation. However, the inclusion of these conditions had several important strengths. In particular, the use of two perturbations in an event-related design reproduced learning in a more realistic practice schedule. Also, the inclusion of "Go" and "NoGo" trials allowed us to dissociate movement- from preparatory-related activity, which is critical but rarely done in imaging studies investigating motor control. Finally, one of the greatest strengths of this study is the use of a relatively novel analytical approach—coherence—to demonstrate the complex systems-level neural interactions, which could not otherwise be appreciated through traditional BOLD analyses techniques.

GRANTS

This work was supported by Public Health Service Grants NS-44393 and NS-33504.

REFERENCES

Aguirre GK, Zarahn E, D'Esposito, M. Empirical analyses of BOLD fMRI statistics. II. Spatially smoothed data collected under null-hypothesis and experimental conditions. *Neuroimage* 5: 199–212, 1997.

Alexander GE, Crutcher MD. Preparation for movement: neural representations of intended direction in three motor areas of the monkey. *J Neurophysiol* 64: 133–150, 1990.

Attwell D, Iadecola C. The neural basis of functional brain imaging signals. *Trends Neurosci* 25: 621–625, 2002.

Barnard ST, Pothen A, Simon H. A spectral algorithm for envelope reduction of sparse matrices. *Numer Linear Algebra Appl* 2: 317–334, 1995.

Blakemore SJ, Sirigu A. Action prediction in the cerebellum and in the parietal lobe. *Exp Brain Res* 153: 239–245, 2003.

Boettiger CA, D'Esposito M. Frontal networks for learning and executing arbitrary stimulus-response associations. *J Neurosci* 25: 2723–2732, 2005.

Chinzei K, Kikinis R, Jolesz F. MR compatibility of mechatronic devices: design criteria. *Proc MICCAI '99 Lecture Notes Comput Sci* 1679: 1020–1031, 1999.

Clower DM, Dum RP, Strick PL. Basal ganglia and cerebellar inputs to "AIP." *Cereb Cortex* 15: 913–920, 2005.

Clower DM, Hoffman JM, Votaw JR, Faber TL, Woods RP, Alexander GE. Role of posterior parietal cortex in the recalibration of visually guided reaching. *Nature* 383: 618–621, 1996.

Clower DM, West RA, Lynch JC, Strick PL. The inferior parietal lobule is the target of output from the superior colliculus, hippocampus, and cerebellum. *J Neurosci* 21: 6283–6291, 2001.

Curtis CE, Sun FT, Miller LM, D'Esposito M. Coherence between fMRI time-series distinguishes two spatial working memory networks. *Neuroimage* 26: 177–183, 2005.

Della-Maggiore V, Malfait N, Ostry D, Paus T. Stimulation of the posterior parietal cortex interferes with arm trajectory adjustments during the learning of new dynamics. *J Neurosci* 24: 9971–9976, 2004.

DeLong MR, Alexander GE, Georgopoulos AP, Crutcher MD, Mitchell SJ, Richardson RT. Role of basal ganglia in limb movements. *Hum Neurobiol* 2: 235–244, 1984a.

DeLong MR, Georgopoulos AP, Crutcher MD, Mitchell SJ, Richardson RT, Alexander GE. Functional organization of the basal ganglia: contributions of single-cell recording studies. *Ciba Found Symp* 107: 64–82, 1984b.

Desmurget M, Epstein CM, Turner RS, Prablanc C, Alexander GE, Grafton ST. Role of the posterior parietal cortex in updating reaching movements to a visual target. *Nat Neurosci* 2: 563–567, 1999.

Desmurget M, Grafton S. Forward modeling allows feedback control for fast reaching movements. *Trends Cogn Sci* 4: 423–431, 2000.

Desmurget M, Grafton ST, Vindras P, Grea H, Turner RS. Basal ganglia network mediates the control of movement amplitude. *Exp Brain Res* 153: 197–209, 2003.

Desmurget M, Grafton ST, Vindras P, Grea H, Turner RS. The basal ganglia network mediates the planning of movement amplitude. *Eur J Neurosci* 19: 2871–2880, 2004.

Desmurget M, Pelisson D, Grethe JS, Alexander GE, Urquizar C, Prablanc C, Grafton ST. Functional adaptation of reactive saccades in humans: a PET study. *Exp Brain Res* 132: 243–259, 2000.

Diedrichsen J, Hashambhoy Y, Rane T, Shadmehr R. Neural correlates of reach errors. *J Neurosci* 25: 9919–9931, 2005.

Diedrichsen J, Verstynen T, Lehman SL, Ivry RB. Cerebellar involvement in anticipating the consequences of self-produced actions during bimanual movements. *J Neurophysiol* 93: 801–812, 2005.

Dreher JC, Grafman J. The roles of the cerebellum and basal ganglia in timing and error prediction. *Eur J Neurosci* 16: 1609–1619, 2002.

Eblen F, Graybiel AM. Highly restricted origin of prefrontal cortical inputs to striosomes in the macaque monkey. *J Neurosci* 15: 5999–6013, 1995.

Floyer-Lea A, Matthews PM. Changing brain networks for visuomotor control with increased movement automaticity. *J Neurophysiol* 92: 2405–2412, 2004.

Fu QG, Mason CR, Flament D, Coltz JD, Ebner TJ. Movement kinematics encoded in complex spike discharge of primate cerebellar Purkinje cells. *Neuroreport* 8: 523–529, 1997.

Garraux G, McKinney C, Wu T, Kansaku K, Nolte G, Hallet M. Shared brain areas but not functional connections controlling movement timing and order. *J Neurosci* 25: 5290–5297, 2005.

Gentilucci M, Negrotti A. Planning and executing an action in Parkinson's disease. *Mov Disord* 14: 69–79, 1999.

Georgopoulos AP, DeLong MR, Crutcher MD. Relations between parameters of step-tracking movements and single cell discharge in the globus pallidus and subthalamic nucleus of the behaving monkey. *J Neurosci* 3: 1586–1598, 1983.

Ghilardi M, Ghez C, Dhawan V, Moeller J, Mentis M, Nakamura T, Antonini A, Eidelberg D. Patterns of regional brain activation associated with different forms of motor learning. *Brain Res* 871: 127–145, 2000.

Graydon FX, Friston KJ, Thomas CG, Brooks VB, Menon RS. Learning-related fMRI activation associated with a rotational visuo-motor transformation. *Brain Res Cogn Brain Res* 22: 373–383, 2005.

Grea H, Pisella L, Rossetti Y, Desmurget M, Tilikete C, Grafton S, Prablanc C, Vighetto A. A lesion of the posterior parietal cortex disrupts on-line adjustments during aiming movements. *Neuropsychologia* 40: 2471–2480, 2002.

Imamizu H, Miyauchi S, Tamada T, Sasaki Y, Takino R, Putz B, Yoshioka T, Kawato M. Human cerebellar activity reflecting an acquired internal model of a new tool. *Nature* 403: 192–195, 2000.

Inoue K, Kawashima R, Satoh K, Kinomura S, Goto R, Sugiura M, Ito M, Fukuda H. Activity in the parietal area during visuomotor learning with optical rotation. *Neuroreport* 8: 3979–3983, 1997.

Inoue, K, Kawashima R, Satoh K, Kinomura S, Sugiura M, Goto R, Ito M, Fukuda H. A PET study of visuomotor learning under optical rotation. *Neuroimage* 11: 505–516, 2000.

Johansen-Berg H, Behrens TE, Robson MD, Drobnjak I, Rushworth MF, Brady JM, Smith SM, Higham DJ, Matthews PM. Changes in connectivity profiles define functionally distinct regions in human medial frontal cortex. *Proc Natl Acad Sci USA* 101: 13335–13340, 2004.

Jueptner M, **Weiller C.** A review of differences between basal ganglia and cerebellar control of movements as revealed by functional imaging studies. *Brain* 121: 1437–1449, 1998.

Kimura M, Matsumoto N, Okahashi K, Ueda Y, Satoh T, Minamimoto T, Sakamoto M, Yamada H. Goal-directed, serial and synchronous activation of neurons in the primate striatum. *Neuroreport* 14: 799–802, 2003.

Krakauer JW, Ghilardi MF, Mentis M, Barnes A, Veytsman M, Eidelberg D, Ghez C. Differential cortical and subcortical activations in learning rotations and gains for reaching: a PET study. *J Neurophysiol* 91: 924–933, 2004.

Lestienne F. Effects of inertial load and velocity on the braking process of voluntary limb movements. *Exp Brain Res* 35: 407–418, 1979.

Logothetis NK. The underpinnings of the BOLD functional magnetic resonance imaging signal." *J Neurosci* 23: 3963–3971, 2003.

Martin TA, Keating JG, Goodkin HP, Bastian AJ, Thach WT. Throwing while looking through prisms. I. Focal olivocerebellar lesions impair adaptation. *Brain* 119: 1183–1198, 1996.

Menon V, Anagnoson RT, Glover GH, Pfefferbaum A. Basal ganglia involvement in memory-guided movement sequencing. *Neuroreport* 11: 3641–3645, 2000.

Messier J, Kalaska JF. Covariation of primate dorsal premotor cell activity with direction and amplitude during a memorized-delay reaching task. *J Neurophysiol* 84: 152–165, 2000.

Miall RC, Jenkinson EW. Functional imaging of changes in cerebellar activity related to learning during a novel eye-hand tracking task. *Exp Brain Res* 166: 170–183, 2005.

Miall RC, Weir DJ, Wolpert DM, Stein JF. Is the cerebellum a Smith predictor? *J Mot Behav* 25: 203–216, 1993.

Miller LM, Sun FT, Curtis CE, D'Esposito M. Functional interactions between oculomotor regions during prosaccades and antisaccades. *Hum Brain Mapp* 26: 119–127, 2005.

Milner TE, **Franklin DW.** Impedance control and internal model use during the initial stage of adaptation to novel dynamics in humans. *J Physiol* 567: 651–664, 2005.

Nezafat R, Shadmehr R, Holcomb HH. Long-term adaptation to dynamics of reaching movements: a PET study. *Exp Brain Res* 140: 66–76, 2001.

Nitschke MF, Stavrou G, Melchert UH, Erdmann C, Peterson D, Wessel K, Heide W. Modulation of cerebellar activation by predictive and non-predictive sequential finger movements. *Cerebellum* 2: 233–240, 2003.

Nixon PD. The role of the cerebellum in preparing responses to predictable sensory events. *Cerebellum* 2: 114–122, 2003.

Osu R, Hirai S, Yoshioka T, Kawato M. Random presentation enables subjects to adapt to two opposing forces on the hand. *Nat Neurosci* 7: 111–112, 2004.

Rencher AC. *Methods of Multivariate Analysis* (2nd ed.). New York: Wiley–Interscience, 2002.

Sergio LE, Hamel-Paquet C, Kalaska JF. Motor cortex neural correlates of output kinematics and kinetics during isometric-force and arm-reaching tasks. *J Neurophysiol* 94: 2353–2378, 2005.

Sergio LE, Kalaska JF. Systematic changes in motor cortex cell activity with arm posture during directional isometric force generation. *J Neurophysiol* 89: 212–228, 2003.

Shadmehr R, Holcomb HH. Neural correlates of motor memory consolidation. *Science* 277: 821–825, 1997.

Shadmehr R, Holcomb HH. Inhibitory control of competing motor memories. *Exp Brain Res* 126: 235–251, 1999.

Smith MA, Shadmehr R. Intact ability to learn internal models of arm dynamics in Huntington's disease but not cerebellar degeneration. *J Neurophysiol* 93: 2809–2821, 2005.

Strick PL, Dum RP, Picard N. Motor areas on the medial wall of the hemisphere. *Novartis Found Symp* 218: 64–75; discussion 75–80; 104–108, 1998.

Sun FT, Miller LM, D'Esposito M. Measuring interregional functional connectivity using coherence and partial coherence analyses of fMRI data. *Neuroimage* 21: 647–658, 2004.

Thoenissen D, Zilles K, Toni I. Differential involvement of parietal and precentral regions in movement preparation and motor intention. *J Neurosci* 22: 9024–9034, 2002.

Timmann D, Richter S, Bestmann S, Kalveram KT, Konczak J. Predictive control of muscle responses to arm perturbations in cerebellar patients. *J Neurol Neurosurg Psychiatry* 69: 345–352, 2000.

Toni I, Passingham RE. Prefrontal-basal ganglia pathways are involved in the learning of arbitrary visuomotor associations: a PET study. *Exp Brain Res* 127: 19–32, 1999.

Toni I, Rowe J, Stephan KE, Passingham RE. Changes of cortico-striatal effective connectivity during visuomotor learning. *Cereb Cortex* 12: 1040–1047, 2002.

Toni I, Rushworth MF, Passingham RE. Neural correlates of visuomotor associations. Spatial rules compared with arbitrary rules. *Exp Brain Res* 141: 359–369, 2001.

Tunik E, Frey SH, Grafton ST. Virtual lesions of the anterior intraparietal area disrupt goal-dependent on-line adjustments of grasp. *Nat Neurosci* 8: 505–511, 2005.

Turner RS, Desmurget M, Grethe J, Crutcher MD, Grafton ST. Motor subcircuits mediating the control of movement extent and speed. *J Neurophysiol* 90: 3958–3966, 2003.

Vaillancourt DE, Mayka MA, Thulborn KR, Corcos DM. Subthalamic nucleus and internal globus pallidus scale with the rate of change of force production in humans. *Neuroimage* 23: 175–186, 2004.

Wichmann T, Bergman H, DeLong MR. The primate subthalamic nucleus. I. Functional properties in intact animals. *J Neurophysiol* 72: 494–506, 1994a.

Wichmann T, Bergman H, DeLong MR. The primate subthalamic nucleus. III. Changes in motor behavior and neuronal activity in the internal pallidum induced by subthalamic inactivation in the MPTP model of parkinsonism. *J Neurophysiol* 72: 521–530, 1994b.